ACS Catalysis

Research Article

pubs.acs.org/acscatalysis

Optimizing the Volmer Step by Single-Layer Nickel Hydroxide Nanosheets in Hydrogen Evolution Reaction of Platinum

Lei Wang,[†] Chong Lin,[†,●] Dekang Huang,[§] Jianmei Chen,[¶] Lin Jiang,[¶] Mingkui Wang,[§] Lifeng Chi,[¶,Δ] Lin Shi,[*,‡] and Jian Jin[*,†]

[†]Nano-Bionics Division and *i*-Lab, [‡]Platforms of Characterization and Test, Suzhou Institute of Nano-Tech and Nano-Bionics, Chinese Academy of Sciences, Suzhou, 215123, China

[¶]Institute of Functional Nano and Soft Materials (FUNSOM), Soochow University, Suzhou, 215123, China

[§]Wuhan National Laboratory for Optoelectronics, Huazhong University of Science and Technology, Wuhan, 430074, China

[Δ]Physikalisches Institut and Center for Nanotechnology (CeNTech), Universität Münster, Münster, 48149, Germany

[●]University of Chinese Academy of Sciences, Beijing, 100049, China

Supporting Information

ABSTRACT: Hydrogen is considered by many to be a promising energy currency, particularly for the transportation sector and for mobile devices. To realize a hydrogen-based fuel economy, hydrogen must be produced in an efficient and sustainable manner. In this article, single-layer nickel hydroxide ($Ni(OH)_2$)-nanosheet-assisted Pt/C catalysis for the hydrogen evolution reaction (HER) in an alkaline environment was investigated. The HER activity trajectories of the hybrid catalysts in correlation with the composition and morphology of $Ni(OH)_2$ were explored in depth. By optimizing the Volmer step through addition of single-layer $Ni(OH)_2$ into Pt/C catalysis, this hybrid catalyst manifests a 110% increase of the HER activity by using only 20 wt % single-layer $Ni(OH)_2$ with a lithium ion additive as compared to the state-of-the-art Pt/C catalyst. Density functional theory calculations revealed that the single-layer $Ni(OH)_2$ behaves superior in adsorption ability of OH^- when compared with multilayer $Ni(OH)_2$. The single-layer $Ni(OH)_2$ contributes to dual improvement on both the Volmer step and the adsorption of OH^- during HER.

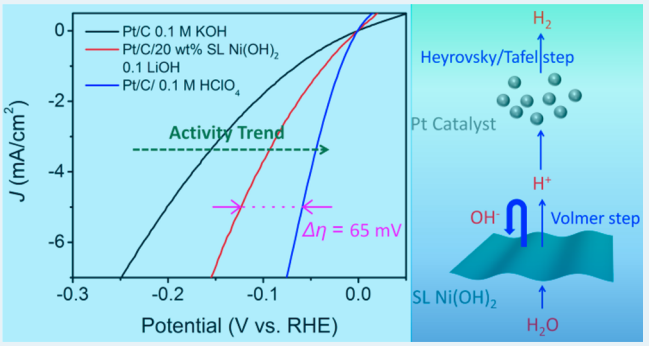

KEYWORDS: *hydrogen evolution reaction, single-layer $Ni(OH)_2$, the Volmer step, density functional theory, $Ni(OH)_2$/Pt composite*

1. INTRODUCTION

The ever-growing concern about environment and energy demands the expansion of renewable energy sources as viable alternatives to fossil-fuel-based technologies, despite several obstacles that need to be overcome, hydrogen is the key energy carrier among these and seems to be one of the most important fuels of the future despite several obstacles still need to be overcome.[1−4] In particular, sustainable hydrogen generated from water splitting via hydrogen evolution reaction (HER) has attracted considerable attention. HER is a multiprocess reaction, and the mechanism of HER is considered to be a combination of three elementary steps including the Volmer step, where water dissociates and a reactive hydrogen intermediate (asorbed hydrogen on the catalyst surface, H_{ad}) is formed, followed by either the Heyrovsky step ($H_2O + H_{ad} + e^- \leftrightarrow H_2 + OH^-$) or the Tafel recombination step ($2H_{ad} \leftrightarrow H_2$).[5,6] Considering that HER is a multistep reaction, the Volmer step and the Heyrovsky/Tafel step are all important to obtaining excellent HER activity.

An advanced catalysis for HER is also required to be able to reduce the overpotential and consequently increase the intrinsic kinetic rate. The intrinsic kinetic rate, defined as the rate at which a reaction proceeds at the equilibrium potential (zero net current), strongly depends on different types of catalysts with several orders of magnitude in variation. The combination of experimental results and theoretical evaluations has been well investigated during the development of advanced electrocatalysts and their surface science from the viewpoint of both fundamental research and practical application. Surface-science-motivated theoretical exploitation provides a significant tool and points to new directions to understand, design and control the surface structure, surface coverage, and surface interaction to enhance electrocatalytical activity.[3] The volcano curve relates the exchange current density (j_o) with the adsorption free energy of the reaction intermediate. Pt is located on the top of the volcano curve and, therefore, is considered the best electrocatalyst for the HER.[7−10] However, Pt is generally inefficient, or not fast enough, for the water dissociation,

Received: November 19, 2014
Revised: May 4, 2015
Published: May 13, 2015

DOI: 10.1021/cs501835c
ACS Catal. 2015, 5, 3801−3806

namely, the Volmer step.[3] In contrast, transition metal (hydro) oxides are effective catalysts for cleaving the HO−H bond, although they are poor at converting the resulting H_{ad} to a hydrogen molecule.[11−18] $Ni(OH)_2$ has been known as the best material for the Volmer step.[19] It could be expected that the Pt hybrid $Ni(OH)_2$ composite will greatly accelerate the speed of a pure Pt catalyst for HER largely. Furthermore, it has been reported that most of metal hydroxides exhibit excellent adsorption abilities for OH^-, generated after the water dissociation by forming H^+ and OH^-.[19] Fast adsorption of OH^- results in fast desorption of OH^- from the Pt surface, which will even further improve the speed of HER. Hence, an optimal route to design a high performance catalyst for HER is to combine fast water dissociation followed with the desorption of OH^- and the efficient recombination of H_{ad} together.[19−21] Unfortunately, to date, a facile method via a wet chemical process to rationally design such an advanced hybrid material and a systematic investigation on the structure/composition−performance relationship are still lacking in the literature.

Herein, we report the fabrication of a single-layer (SL) $Ni(OH)_2$-Pt/C (platinum nanoparticles supported on XC-72 carbon) hybrid catalyst with superior HER activity. SL $Ni(OH)_2$, with the thickness around 1 nm, is a two-dimensional (2D) single-molecule metal hydroxide layer where all of the atoms (e.g., active sites for dissociation of water and adsorption of OH^-) are exposed on the surface. By designing the SL $Ni(OH)_2$-Pt/C catalyst, the hybrid structure could maximize the efficiency of water dissociation and adsorption of OH^-, and reduce the pure weight of the Pt catalyst. In this work, both the SL $Ni(OH)_2$ and multilayer (ML) $Ni(OH)_2$-Pt/C hybrid catalysts are prepared and investigated by experiments and theories. As a result, the SL $Ni(OH)_2$-Pt/C hybrid catalyst manifests a 41% increase of HER activity when compared to the state-of-the-art Pt/C catalysts by using only 20 wt % SL $Ni(OH)_2$. In addition, the activity can be further enhanced via Li^+-induced destabilization of the HO−H bond, resulting in a 110% increase of HER activity. The DFT calculation further demonstrates that SL $Ni(OH)_2$ exhibits a more negative binding energy than ML $Ni(OH)_2$ for the adsorption of OH^-.

2. EXPERIMENTAL SECTION

Materials. Nickel(II) nitrate hexahydrate ($Ni(NO_3)_2 \cdot 6H_2O$) (99.999% trace metals basis), sodium dodecyl sulfate (SDS) (≥99.0%), KOH solution (1 M), Nafion solution, and hexamethylenetetramine (HMT) (≥99.0%) were purchased from Sigma-Aldrich. Platinum, nominally 20 wt % on carbon black (Pt/C), and formamide (≥99.5%) were purchased from Alfa Aesar. All the chemicals were used as received without further purification. All gases (argon and hydrogen) (99.999%) were purchased from Jin-Hong company. Water was purified immediately before use in a Millipore Direct-Q system.

Characterizations. Scanning electron microscopy (SEM) was measured on a Quanta 400 FEG field-emission scanning electron microscope. Transmission electron microscopy (TEM) was measured on a Tecnai G2 F20 S-Twin field-emission transmission electron microscope. X-ray diffraction (XRD) was collected on a Bruke D8. Electrochemical measurements were performed by Autolab PGSTAT302N.

Preparation of ML and SL $Ni(OH)_2$. For the preparation of ML $Ni(OH)_2$, $Ni(NO_3)_2 \cdot 6H_2O$, sodium dodecyl sulfate (SDS), and hexamethylenetetramine (HMT) were dissolved in 50 mL of deionized water to give the final concentrations of 5, 20, and 15 mM in a Teflon beaker. Each solution was then filled with nitrogen gas and heated to 120 °C for 12 h. After the reaction, the product was filtered and washed with deionized water and anhydrous ethanol several times, and finally air-dried at room temperature. For the preparation of SL $Ni(OH)_2$, 0.2 g of as-prepared ML $Ni(OH)_2$ was mixed with 200 mL of formamide and stirred under nitrogen protection for 48 h at 60 °C. To purify the exfoliated product, the resulting solution was centrifuged at 8000 rpm for 10 min in order to remove the nonexfoliated parts. Inductive coupled plasma emission spectrometer-atomic emission spectrometer (ICP-AES) was carried out on a Vista AX for testing the resulting products.

Considering the process for the preparation of ML $Ni(OH)_2$ that involves the use of SDS, a small amount of dodecyl sulfate (DS) anions could coordinate with part of the nickel, and a small amount of crystalliferous water and interlayer water might exist in $Ni(OH)_2$. In order to quantify the net weight of $Ni(OH)_2$ precisely, ICP-AES was used to determine the net weight of $Ni(OH)_2$. The result showed that the net weight of ML $Ni(OH)_2$ in the as-prepared product was 68 wt %, and the residue 32 wt % was contributed by DS anion, interlayer water, and crystalliferous water.

Electrochemical Characterization. Before the preparation of catalyst inks for HER, the concentration of ML and SL $Ni(OH)_2$ in ethanol and formamide dispersion, respectively, were first adjusted by ICP-AES measurements to give a final concentration of 0.5 mg/mL. All electrochemical characterizations were conducted in an electrochemical cell using Ag/AgCl (filled with 3 M KCl) as reference electrode, a platinum rod as the counter electrode, and the sample modified glassy carbon rotating disk electrode (GC-RDE) (diameter is 3 mm) as the working electrode. All polarization curves were corrected by current-resistance (*iR*) compensation within the cell. All the experiments were scanned at a speed of 50 mV/s. All potentials were calibrated with respect to reversible hydrogen electrode (RHE).

HER Measurement. Two milligrams of Pt/C (containing 0.4 mg Pt) was mixed with a certain amount of ML or SL $Ni(OH)_2$ dispersion to give the mass ratio of Pt/ML or SL $Ni(OH)_2$ of 1:0, 8:1, 4:1, 2:1, 1:1, and 1:2. All catalyst inks were diluted to 10 mL by adding ethanol and 200 μL of Nafion solution (5%). After ultrasonication for 30 min to form a homogeneous dispersion, 2 μL of the catalyst ink was loaded on the GC-RDE. The Pt loaded on the GC-RDE was calculated to be 1.13 $\mu g/cm^2$. It is worthy to note that the use of a small loading amount of catalyst is to avoid significant bubble formation during the test. The ink was dried for 12 h in air at 70 °C to give a uniform thin film at RDE surface. In each experiment, the electrode was immersed in a solution saturated with Ar at 0.05 V. After obtaining a stable cycle between 0.05 and 0.7 V, the electrolyte was saturated with H_2 and subsequently polarization curves for HER were recorded on the RDE between 0.1 and −0.3 V. Cyclic voltammetry (CV) curves were recorded from 0.05 to 1 V in an H_2 saturated electrolyte at the scan rate of 50 mV/s. All polarization curves were collected at the rotating speed of 1600 rpm.

DFT Calculation. DFT was carried out by employing fully periodic plane-wave DFT calculations, using the Vienna Ab-initio Simulation Package (VASP).[22] Electron exchange and correlation were described within the PW91 generalized gradient approximation (GGA),[23,24] and the Projector Augmented Wavefuction (PAW) methods[25,26] were also used. For Ni calculations, Hubbard U correction was used. The applied U values for Ni calculations involving $Ni(OH)_2$ films

DOI: 10.1021/cs501835c
ACS Catal. 2015, 5, 3801−3806

was 4.216 eV.[27] A slab with a 2 × 2 (corresponding to 1/4 molecular layer coverage) surface unit cell and about 15 Å of vacuum between any two slabs was used. A 400 eV cutoff for the kinetic energy of the plane-wave basis-set was used. The first Brillouin zone was sampled with a 2 × 2 × 1 Monkhorst–Pack k-point mesh. Total electronic energies were converged to 10^{-5} eV and forced to 0.02 eV/Å.

3. RESULTS AND DISCUSSION

3.1. Preparation and Structure Characterization of SL Ni(OH)$_2$-Pt/C Hybrid Catalyst. SL Ni(OH)$_2$, ML Ni(OH)$_2$ was synthesized according to our previous report with slight modifications.[28,29] The as-prepared ML Ni(OH)$_2$ shows a sheet-like morphology with thickness of tens of nanometers (see Supporting Information, Figure S1). The XRD pattern demonstrates its layered structure with an interlayer spacing of 1.6 nm (Figure S2, and see Supporting Information for detailed calculations). The exfoliation of ML Ni(OH)$_2$ into SL Ni(OH)$_2$ was conducted in formamide with heat assistance. The obtained SL Ni(OH)$_2$ was examined by transmission electron microscopy (TEM) and atomic force microscopy (AFM). As shown in Figure 1a, the sheet-like structures with

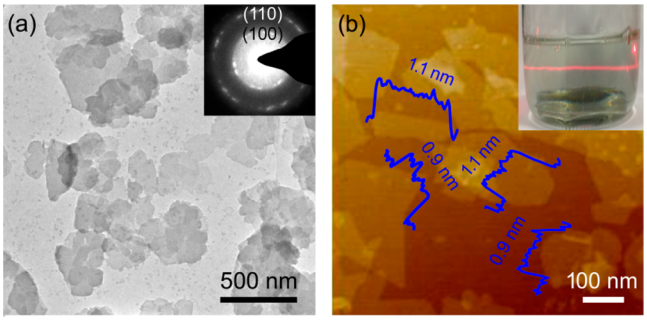

Figure 1. Structure characterization of SL Ni(OH)$_2$. (a) TEM and SAED (inset of a) images. AFM image (b) and corresponding height profile. Inset of panel b shows SL Ni(OH)$_2$ dispersion.

lateral size from several tens to several hundred nanometers are clearly seen. The thickness of the sheets is 1 ± 0.2 nm, which is in agreement with our previous report.[30] The selected area electron diffraction (SAED) image taken from the sheets demonstrates two bright diffraction circles, which correspond to the (100) and (110) planes of SL Ni(OH)$_2$ (inset of Figure 1a). Clear Tyndall light scattering is discerned for SL Ni(OH)$_2$ dispersion with a light-green color, indicating the presence of well-dispersed colloidal sheets (inset of Figure 1b).

The SL Ni(OH)$_2$-Pt/C hybrid catalyst was prepared by adding different amounts of a SL Ni(OH)$_2$ dispersion into a Pt/C dispersion and ultrasonicated for at least 30 min to form a homogeneous black ink. The SL Ni(OH)$_2$ is positively charged with zeta potential of 56.5 mV (see Supporting Information, Figure S9), while the Pt nanoparticles are commonly negatively charged. The different charging between Pt nanoparticles and SL Ni(OH)$_2$ causes the effective contact between them driven by electrostatic forces.[31] Different from the pure Pt/C catalyst (Figure 2a), the curled structure of SL Ni(OH)$_2$ could be clearly seen in the mixture of SL Ni(OH)$_2$ and Pt/C, which is due to the electrostatic attraction between Pt nanoparticles and SL Ni(OH)$_2$. The SL Ni(OH)$_2$ encapsulated Pt/C shows crinkled and rough textures, associated with the presence of ultrathin SL Ni(OH)$_2$. The edge of individual as well as

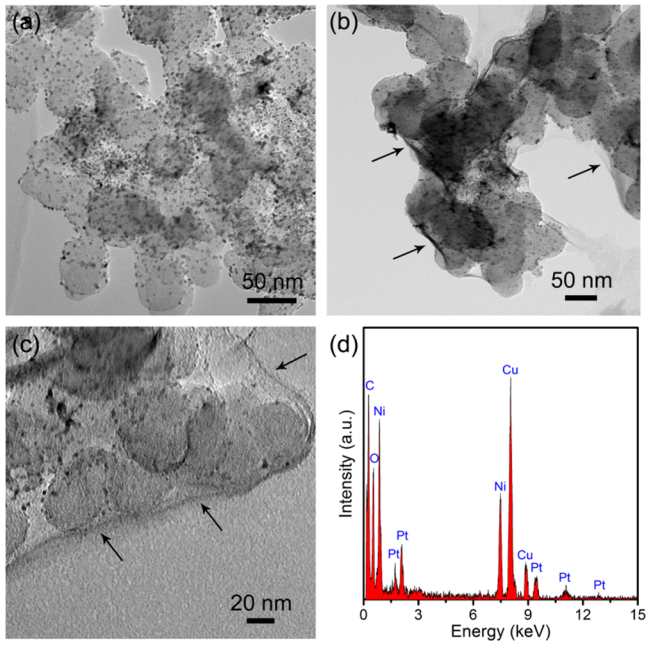

Figure 2. (a) TEM image of commercial Pt/C (20 wt % of Pt) catalyst. (b) TEM image and (c) high-magnification TEM image of SL Ni(OH)$_2$-Pt/C hybrid catalyst. (d) Corresponding EDS profile. Black arrows in (b) and (c) indicate the presence of SL Ni(OH)$_2$ in sheet-like structure.

overlapping SL Ni(OH)$_2$ could be clearly observed as indicated by black arrows in Figure 2b,c. The black dots with diameters ranging from 2 to 4 nm in the figures are Pt nanoparticles. The corresponding energy dispersive spectrometer (EDS) profile indicates the presence of SL Ni(OH)$_2$ as shown in Figure 2d.

3.2. HER Activity of Ni(OH)$_2$-Pt/C Hybrid Catalysts. The HER activity of both ML Ni(OH)$_2$-Pt/C hybrid catalysts and SL Ni(OH)$_2$-Pt/C hybrid catalysts with different weight percentages of Ni(OH)$_2$ were measured. Figure 3a shows the

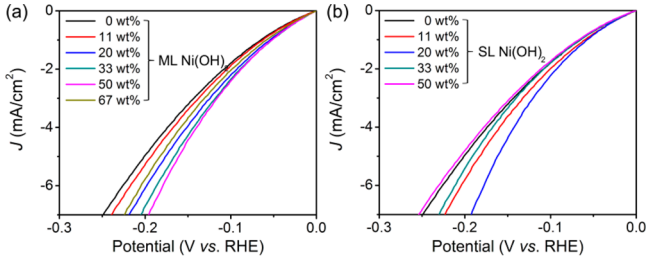

Figure 3. Polarization curves of (a) ML Ni(OH)$_2$-Pt/C hybrid catalysts and (b) SL Ni(OH)$_2$-Pt/C hybrid catalysts with various weight percentage of Ni(OH)$_2$ at the scan rate of 50 mV/s in H$_2$-saturated KOH (0.1 M).

polarization curves of ML Ni(OH)$_2$-Pt/C hybrid catalysts with different weight percentages of Ni(OH)$_2$. To avoid significant bubble formation during the test, the amount of Pt loaded on the RDE was 1.13 μg/cm^2, and the potential limits are −0.3 V versus reverse hydrogen electrode (RHE) in this work. Although the weight of the catalyst is low, the background signal coming from the glass carbon is negligible (see Supporting Information, Figure S4). As shown in Figure 3a, the HER activity obviously increases with an increase in the amount of ML Ni(OH)$_2$ from 11 wt % to 50 wt %. The

DOI: 10.1021/cs501835c
ACS Catal. 2015, 5, 3801−3806

overpotential of the ML $Ni(OH)_2$ (50 wt %)-Pt/C hybrid catalyst decreased 39 mV when compared with pure Pt/C catalyst; further increasing the amount of ML $Ni(OH)_2$ will decrease the HER activity. A 184 mV overpotential at a current density of 5 mA/cm^2 is obtained when the amount of ML $Ni(OH)_2$ is 67 wt %. $Ni(OH)_2$ could indeed act as an effective water dissociation catalyst; an appropriate amount of ML $Ni(OH)_2$ could accelerate water dissociation and improve HER activity in contrast to pure Pt/C catalyst. However, excess $Ni(OH)_2$ will block the active sites on Pt to play a role in the H_{ad} recombination step and give rise to a lower HER activity.

Figure 3b is the polarization curves of the SL $Ni(OH)_2$-Pt/C hybrid catalysts with different weight percentages of SL $Ni(OH)_2$. It shows that the HER activity increases greatly by increasing the amount of SL $Ni(OH)_2$ up to 20 wt % with an overpotential of 157 mV at a current density of 5 mA/cm^2. In this case, the overpotential decreases 42 mV in comparison to a pure Pt/C catalyst. At the overpotential of 150 mV, a current density of 4.52 mA/cm^2 is obtained, which corresponds to a 41% increase of the HER activity when compared to the state-of-the-art Pt/C catalyst (3.2 mA/cm^2). Further increasing the amount of SL $Ni(OH)_2$ decrease the HER activity of the hybrid catalyst quickly. When the amount of SL $Ni(OH)_2$ increases to 50 wt %, it shows a lower activity than pure Pt/C. Obviously, SL $Ni(OH)_2$ is more efficient than ML $Ni(OH)_2$ for water dissociation. A 20 wt % SL $Ni(OH)_2$ in the hybrid catalyst gives an optimum HER activity.

To investigate the HER activity trajectories of the hybrid catalysts correlated with the composition and morphology of $Ni(OH)_2$ in depth, cyclic voltammetry (CV) measurements in H_2-saturated electrolyte were carried out. CV curves of both ML $Ni(OH)_2$-Pt/C hybrid catalysts and SL $Ni(OH)_2$-Pt/C hybrid catalysts exhibit the electrochemical characteristic of Pt as shown in Figure 4a,b. By increasing the amount of $Ni(OH)_2$, the area of the H_{upd} (defined as the adsorption of under-potentially deposited hydrogen) decreases in both of the two cases.[32] The electrochemical surface area (ECSA) was

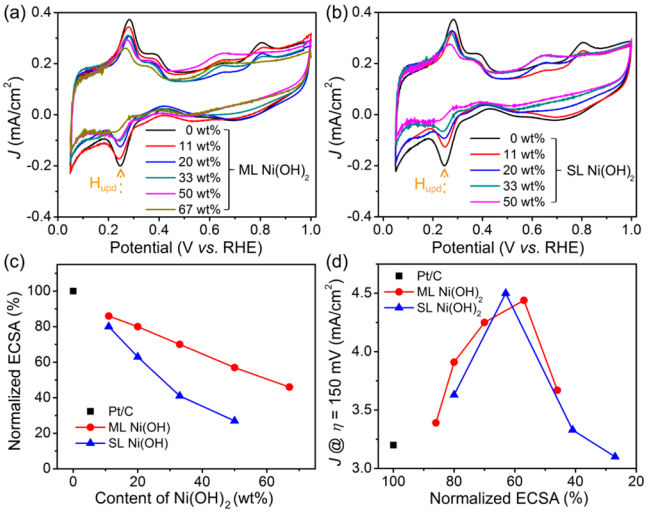

Figure 4. CV curves of (a) ML $Ni(OH)_2$-Pt/C hybrid catalysts and (b) SL $Ni(OH)_2$-Pt/C hybrid catalysts with different weight percentages of $Ni(OH)_2$ at the scan rate of 50 mV/s in H_2-saturated KOH (0.1 M). (c) Variation of normalized ECSA with different weight percentages of $Ni(OH)_2$. (d) Plots of normalized ECSA versus current density at the overpotential of 150 mV.

calculated by integrating the area for hydrogen adsorption region from 0.05 to 0.4 V in the CV curves to investigate the influence of $Ni(OH)_2$ (see Supporting Information, Figure S5).[32,33] The relationship between the amount of $Ni(OH)_2$ and ECSA for both the ML $Ni(OH)_2$ and SL $Ni(OH)_2$-Pt/C hybrid catalysts are studied first. The normalized ECSA (based on pure Pt/C) versus the amount of $Ni(OH)_2$ are plotted in Figure 4c. By increasing the amount of $Ni(OH)_2$, the ECSA decreases for both the ML $Ni(OH)_2$ and SL $Ni(OH)_2$-Pt/C hybrid catalysts. However, they show different declining trends where the SL $Ni(OH)_2$-Pt/C hybrid catalysts exhibit much faster declining trend than ML $Ni(OH)_2$-Pt/C hybrid catalysts. This is because SL $Ni(OH)_2$ is a 2D single-molecule metal hydroxide layer with the thickness of only 1 nm and possesses an inherently high specific area. It could provide higher utilization for the $Ni(OH)_2$-Pt/C hybrid catalyst than ML $Ni(OH)_2$. As shown in Figure 4c, only 20 wt % SL $Ni(OH)_2$ reduces 37% of the ECSA for the SL $Ni(OH)_2$-Pt/C hybrid catalyst, indicating high utilization of $Ni(OH)_2$. The same reduction of ECSA could be obtained in the ML $Ni(OH)_2$-Pt/C hybrid catalyst by using about 42 wt % ML $Ni(OH)_2$. Figure 4d summarizes the normalized ECSA versus current density (at the overpotential of 150 mV) plots of the ML $Ni(OH)_2$ and SL $Ni(OH)_2$-Pt/C hybrid catalysts. Both of the ML and SL $Ni(OH)_2$ based hybrid catalysts exhibit the best catalytic activity when the ECSA is around 60%. With the decrease of ECSA (that is, increasing the amount of $Ni(OH)_2$), both of the two kinds of catalysts show decreased activity. In addition, when the ECSA is down to 27% in the SL $Ni(OH)_2$-Pt/C hybrid catalyst, the activity of the SL $Ni(OH)_2$-Pt/C hybrid catalyst is lower than that of the pure Pt/C catalyst. Considering the dual-function of the $Ni(OH)_2$-Pt/C hybrid catalyst to catalytic activity, the reaction rates should be directly proportional to the number of active sites. Increasing the amount of $Ni(OH)_2$ will enhance the speed of water dissociation due to the increase in activity sites that are provided by $Ni(OH)_2$. However, the speed of H_{ad} recombination might be reduced due to the loss of ECSA that is generated by Pt. Therefore, there is a balance between $Ni(OH)_2$ and Pt, that is, the balance of catalytic efficiency between water dissociation and recombination of H_{ad}. As has been demonstrated above, the best catalytic activity for the $Ni(OH)_2$-Pt/C hybrid system is obtained when the ECSA is around 60% for both ML and SL $Ni(OH)_2$. By use of SL $Ni(OH)_2$, the weight of $Ni(OH)_2$ could be reduced to be 20 wt %, much lower than ML $Ni(OH)_2$ (50 wt %).

To further enhance the HER activity of the SL $Ni(OH)_2$-Pt/C hybrid catalyst, 0.1 M LiOH was used as the electrolyte. It is well-known that Li^+ can interact with water and display stronger OH_{ad} than K^+ in an alkaline environment.[34] As shown in Figure 5a, the SL $Ni(OH)_2$ (20 wt %)-Pt/C hybrid catalyst exhibits enhanced HER activity in 0.1 M LiOH electrolyte. The overpotential decreases to 121 mV at a current density of 5 mA/cm^2. It equals a 79 mV decrease of the overpotential when compared to Pt/C (Figure 5b). At the overpotential of 150 mV, a current density of 6.6 mA/cm^2 is obtained, which corresponds to a 110% increase in HER activity, demonstrating greatly enhanced performance when compared to the state-of-the-art Pt/C catalyst. Furthermore, at 5 mA/cm^2, the difference in overpotential between Pt/C in acid solution (0.1 M $HClO_4$) and SL $Ni(OH)_2$-Pt/C in alkaline solution (0.1 M LiOH) narrows to 65 mV.

3.3. DFT Calculation. The Volmer step in HER through water splitting in alkaline media is of central importance. As

DOI: 10.1021/cs501835c
ACS Catal. 2015, 5, 3801−3806

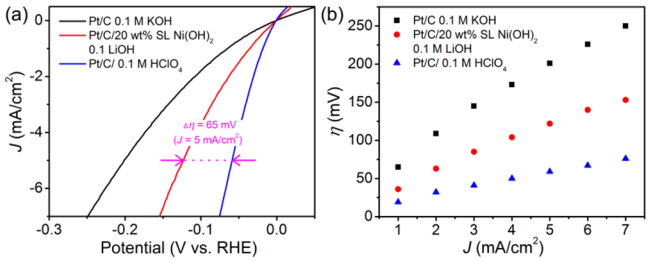

Figure 5. (a) Polarization curves at the scan rate of 50 mV and (b) plots of current density versus overpotential for Pt/C and SL $Ni(OH)_2$ (20 wt %)-Pt/C hybrid catalyst in 0.1 M KOH and SL $Ni(OH)_2$ (20 wt %)-Pt/C hybrid catalyst in 0.1 M LiOH, respectively.

shown by the above results, the activities of commercial Pt/C for HER in alkaline are largely enhanced by adding $Ni(OH)_2$, either SL or ML. In our hybrid catalysts, the SL/ML $Ni(OH)_2$ first promotes the dissociation of water and then H^+ is adsorbed on the nearby Pt and OH^- is adsorbed on the SL/ML $Ni(OH)_2$. Besides a big difference in the specific surface area between SL and ML $Ni(OH)_2$, their electronic structures might also be different, which may cause a different effect on adsorption of OH^- when considering the single layer structure of SL $Ni(OH)_2$. To further investigate the different binding energy for OH^- (denoted as $BE_{(OH)}$) between ML and SL $Ni(OH)_2$, DFT calculations were used to identify the absorption energy of OH^- on the surface of SL and ML $Ni(OH)_2$, and a Hubbard U correction was used. It is worthy to note that such a correction has been proven to be useful in improving the DFT description of electron correlation in transition metal hydroxides, in particular when the localization of charge carriers (electrons and holes) is involved.[35,36] To calculate the OH^- binding energy on SL or ML $Ni(OH)_2$, one OH^- group is removed to create an OH^- vacancy (denoted as OH_v) (for ML $Ni(OH)_2$, six molecular layers are built and one OH^- group is removed from the top layer to create a OH_v), and the initializations of atoms are relaxed into the lowest energy configurations[37] as shown in Figure 6a,c. The $BE_{(OH)}$ is calculated as follows: $BE_{(OH)} = E_{(Ni(OH)_2)} - E_{(Ni(OH)_2-OH_v)} - [E_{(H_2O)} - 0.5E_{(H_2)}]$, where $E_{(Ni(OH)_2)}$ is the total energy of the $Ni(OH)_2$, $E_{(Ni(OH)_2-OH_v)}$ is the energy of $Ni(OH)_2$ with an OH_v, and $E_{(H_2O)}$ and $E_{(H_2)}$ are the energies of H_2O and H_2 in gas phase. The results show that the $BE_{(OH)}$ of SL $Ni(OH)_2$ is −1.12 eV, more negative than ML $Ni(OH)_2$, which is −1.04 eV (Figure 6b,d) (see Supporting Information for detailed calculations). In principle, the more negative $BE_{(OH)}$ is, the stronger the OH^- binds to $Ni(OH)_2$. Clearly, SL $Ni(OH)_2$ possesses an enhanced binding ability to OH^- when compared to ML $Ni(OH)_2$. Based on the above ECSA analysis and DFT calculation, we conclude that the SL $Ni(OH)_2$ could not only improve the efficiency of Volmer step more than ML $Ni(OH)_2$ but also exhibit a better ability for the adsorption of OH^- during the HER. These two advantages contribute to the speed acceleration of the entire HER.

The HER in alkaline environment, serving as a model reaction for exploring the relationship between the electrode materials and the kinetic rates of electrochemical transformation of water into a hydrogen molecule, is of considerable importance from fundamental research. In all of the catalysts for the HER, Pt offers the highest activity and stability. However, as a scarce resource, the high price of Pt is always a

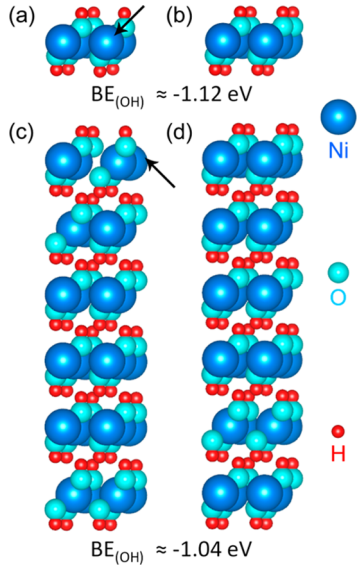

Figure 6. Side view of the structure of (a) SL $Ni(OH)_2$ and (c) ML $Ni(OH)_2$ with an OH_V (pointed by the black arrows), respectively. Side view of the structure of (b) SL $Ni(OH)_2$ and (d) ML $Ni(OH)_2$ with an OH_V after the adsorption of the OH^- groups.

hurdle for a wider practical application. Alternatively to Pt, high-surface-area Raney Ni and Ni alloys as conventional alkaline water electrolyzers are also used.[38] These materials are cheaper but not active enough. It thus provides a significant scope for improving the reaction kinetics at the cathode. Nowadays, with the development of nanotechnology, various metal oxide/sulfides with ultrafine structures have been prepared and used for HER.[39−46] Unfortunately, none of these materials could exceed or approach the activity of Pt. On this basis, exploring a well-controlled and solution-processed method to optimize the structure and composition of the Pt/$Ni(OH)_2$ hybrid becomes rather necessary to achieve the best HER activity. From another point of view, enhancing the HER activity of Pt/non-noble metal hybrid catalysts also means decreasing the amount of Pt loading under the same condition.

4. CONCLUSIONS

In summary, an improved hydrogen evolution activity of Pt assisted by $Ni(OH)_2$ was reported in this work. The $Ni(OH)_2$-Pt/C hybrid catalysts were prepared in a wet chemical process. The HER activity trajectories of the hybrid catalysts correlated with a different composition and structure of $Ni(OH)_2$ were systematically investigated by both experiments and theory. The hybrid catalysts demonstrated greatly enhanced HER activity with the assistance of SL $Ni(OH)_2$ nanosheets, superior to the state-of-the-art Pt/C catalyst. Our work provides a new technology to design high-performance Pt-based hybrid catalysts by a facile method. This strategy could be further expanded to the design of other catalysis reactions that start from water dissociation process such as oxygen evolution reaction.

■ ASSOCIATED CONTENT

Supporting Information

The Supporting Information is available free of charge on the ACS Publications website at DOI: 10.1021/cs501835c.

DOI: 10.1021/cs501835c
ACS Catal. 2015, 5, 3801−3806

Materials and experimental section, characterization of ML $Ni(OH)_2$, ECSA calculation, cyclic performance of catalyst, details of DFT calculation (PDF)

AUTHOR INFORMATION

Corresponding Authors

*E-mail: jjin2009@sinano.ac.cn.
*E-mail: lshi2007@sinano.ac.cn.

Notes

The authors declare no competing financial interest.

ACKNOWLEDGMENTS

We would like to thank Dr. Michael J. Giroux from the Department of Chemical and Biomolecular Engineering, Johns Hopkins University for his help with English polishing for the manuscript. This work was supported by the National Natural Science Foundation of China (No. 21433012, 11374328), the Key Development Project of Chinese Academy of Sciences (No. KJZD-EW-M01-3), the National Basic Research Program of China (No. 2013CB933000), and the Natural Science Foundation of Jiangsu Province (No. BK20130007). We are grateful for the professional services offered by the Platforms of Characterization and Test at Suzhou Institute of Nano-Tech and Nano-Bionics (SINANO), and Supercomputing Center, Computer Network Information Center (CNIC) at Chinese Academy of Sciences (CAS).

REFERENCES

(1) Greeley, J.; Jaramillo, T. F.; Bonde, J.; Chorkendorff, I.; Nørskov, J. K. *Nat. Mater.* **2006**, *5*, 909−913.
(2) Chu, S.; Majumdar, A. *Nature* **2012**, *488*, 294−303.
(3) Greeley, J.; Markovic, N. M. *Energy Environ. Sci.* **2012**, *5*, 9246−9256.
(4) Koper, M. T. M. *Nat. Chem.* **2013**, *5*, 255−256.
(5) Bockris, J. O'M.; Potter, E. C. *J. Electrochem. Soc.* **1952**, *99*, 169−186.
(6) Sheng, W.; Gasteiger, H. A.; Shao-Horn, Y. *J. Electrochem. Soc.* **2010**, *157*, B1529−B1536.
(7) Nørskov, J. K.; Bligaard, T.; Logadottir, A.; Kitchin, J. R.; Chen, J. G.; Pandelov, S.; Stimming, U. *J. Electrochem. Soc.* **2005**, *152*, J23−J26.
(8) Skúlason, E.; Karlberg, G. S.; Rossmeisl, J.; Bligaard, T.; Greeley, J.; Jónsson, H.; Nørskov, J. K. *Phys. Chem. Chem. Phys.* **2007**, *9*, 3241−3250.
(9) Strmcnik, D.; Tripkovic, D.; van der Vliet, D.; Stamenkovic, V.; Markovic, N. M. *Electrochem. Commun.* **2008**, *10*, 1602−1605.
(10) Yu, W.; Porosoff, M. D.; Chen, J. G. *Chem. Rev.* **2012**, *112*, 5780−5817.
(11) Hinnemann, B.; Moses, P. G.; Bonde, J.; Jørgensen, K. P.; Nielsen, J. H.; Horch, S.; Chorkendorff, I.; Nørskov, J. K. *J. Am. Chem. Soc.* **2005**, *127*, 5308−5309.
(12) Jaramillo, T. F.; Jørgensen, K. P.; Bonde, J.; Nielsen, J. H.; Horch, S.; Chorkendorff, I. *Science* **2007**, *317*, 100−102.
(13) Esposito, D. V.; Hunt, S. T.; Stottlemyer, A. L.; Dobson, K. D.; Mccandless, B. E.; Birkmire, R. W.; Chen, J. G. *Angew. Chem., Int. Ed.* **2010**, *49*, 9859−9862.
(14) Li, Y.; Wang, H.; Xie, L.; Liang, Y.; Hong, G.; Dai, H. *J. Am. Chem. Soc.* **2011**, *133*, 7296−7299.
(15) Xu, Y.; Gao, M.; Zheng, Y.; Jiang, J.; Yu, S. *Angew. Chem., Int. Ed.* **2013**, *52*, 8546−8550.
(16) Voiry, D.; Yamaguchi, H.; Li, J.; Silva, R.; Alves, D. C. B.; Fujita, T.; Chen, M.; Asefa, T.; Shenoy, V. B.; Eda, G.; Chhowalla, M. *Nat. Mater.* **2013**, *12*, 850−855.
(17) Zeng, Z.; Tan, C.; Huang, X.; Bao, S.; Zhang, H. *Energy Environ. Sci.* **2014**, *7*, 797−803.
(18) Huang, X.; Zeng, Z.; Bao, S.; Wang, M.; Qi, X.; Fan, Z.; Zhang, H. *Nat. Commun.* **2013**, *4*, 1444−1451.
(19) Subbaraman, R.; Tripkovic, D.; Strmcnik, D.; Chang, K.; Uchimura, M.; Paulikas, A. P.; Stamenkovic, V.; Markovic, N. M. *Science* **2011**, *334*, 1256−1260.
(20) Danilovic, N.; Subbaraman, R.; Strmcnik, D.; Chang, K.; Paulikas, A. P.; Stamenkovic, V. R.; Markovic, N. M. *Angew. Chem., Int. Ed.* **2012**, *51*, 12495−12498.
(21) Strmcnik, D.; Uchimura, M.; Wang, C.; Subbaraman, R.; Danilovic, N.; van der Vliet, D.; Paulikas, A. P.; Stamenkovic, V. R.; Markovic, N. M. *Nat. Chem.* **2013**, *5*, 300−306.
(22) Kresse, G.; Furthmüller, J. *Phys. Rev. B: Condens. Matter Mater. Phys.* **1996**, *54*, 11169−11186.
(23) White, J. A.; Bird, D. M. *Phys. Rev. B: Condens. Matter Mater. Phys.* **1994**, *50*, 4954−4957.
(24) Perdew, J. P.; Chevary, J. A.; Vosko, S. H.; Jackson, K. A.; Pederson, M. R.; Singh, D. J.; Fiolhais, C. *Phys. Rev. B: Condens. Matter Mater. Phys.* **1992**, *46*, 6671−6687.
(25) Blöchl, P. E. *Phys. Rev. B: Condens. Matter Mater. Phys.* **1994**, *50*, 17953−17979.
(26) Kresse, G.; Joubert, D. *Phys. Rev. B: Condens. Matter Mater. Phys.* **1999**, *59*, 1758−1775.
(27) Solovyev, I. V.; Dederichs, P. H.; Anisimov, V. I. *Phys. Rev. B: Condens. Matter Mater. Phys.* **1994**, *50*, 16861−16871.
(28) Wang, L.; Dong, Z.; Wang, Z.; Zhang, F.; Jin, J. *Adv. Funct. Mater.* **2013**, *23*, 2758−2764.
(29) Wang, L.; Lin, C.; Zhang, F.; Jin, J. *ACS Nano* **2014**, *8*, 3724−3734.
(30) Wang, L.; Lin, C.; Huang, D.; Zhang, F.; Wang, M.; Jin, J. *ACS Appl. Mater. Interfaces* **2014**, *6*, 10172−10180.
(31) Wang, L.; Wang, D.; Dong, X.; Zhang, Z.; Pei, X.; Chen, X.; Chen, B.; Jin, J. *Chem. Commun.* **2011**, *47*, 3556−3558.
(32) Wang, D.; Xin, H. L.; Hovden, R.; Wang, H.; Yu, Y.; Muller, D. A.; Disalvo, F. J.; Abruña, H. D. *Nat. Mater.* **2013**, *12*, 81−87.
(33) Cui, C.; Gan, L.; Heggen, M.; Rudi, S.; Strasser, P. *Nat. Mater.* **2013**, *12*, 765−771.
(34) Strmcnik, D.; Kodama, K.; van der Vliet, D.; Greeley, J.; Stamenkovic, V. R.; Markovic, N. M. *Nat. Chem.* **2009**, *1*, 466−472.
(35) Nørskov, J. K.; Bligaard, T.; Rossmeisl, J.; Christensen, C. H. *Nat. Chem.* **2009**, *1*, 37−46.
(36) Bajdich, M.; García-Mota, M.; Vojvodic, A.; Nørskov, J. K.; Bell, A. T. *J. Am. Chem. Soc.* **2013**, *135*, 13521−13530.
(37) Subbaraman, R.; Tripkovic, D.; Chang, K.; Strmcnik, D.; Paulikas, A. P.; Hirunsit, P.; Chan, M.; Greeley, J.; Stamenkovic, W.; Markovic, N. M. *Nat. Mater.* **2012**, *11*, 550−557.
(38) Birry, L.; Lasia, A. *J. Appl. Electrochem.* **2004**, *34*, 735−749.
(39) Hinnemann, B.; Moses, P. G.; Bonde, J.; Jørgensen, K. P.; Nielsen, J. H.; Horch, S.; Chorkendorff, I.; Nørskov, J. K. *J. Am. Chem. Soc.* **2005**, *127*, 5308−5309.
(40) Wang, H.; Lu, Z.; Xu, S.; Kong, D.; Cha, J. J.; Zheng, G.; Hsu, P.; Yan, K.; Bradshaw, D.; Prinz, F. B.; Cui, Y. *Proc. Natl. Acad. Sci. U. S. A.* **2014**, *110*, 19701−19706.
(41) Lukowski, M. A.; Daniel, A. S.; Meng, F.; Forticaux, A.; Li, L.; Jin, S. *J. Am. Chem. Soc.* **2013**, *135*, 10274−10277.
(42) Vrubel, H.; Hu, X. *Angew. Chem., Int. Ed.* **2012**, *51*, 12703−12706.
(43) Voiry, D.; Yamaguchi, H.; Li, J.; Silva, R.; Alves, D. C. B.; Fujita, T.; Chen, M.; Asefa, T.; Shenoy, V. B.; Eda, G.; Chhowalla, M. *Nat. Mater.* **2013**, *12*, 850−855.
(44) Le Goff, A.; Artero, V.; Jousselme, B.; Tran, P. D.; Guillet, N.; Métayé, R.; Fihri, A.; Palacin, S.; Fontecave, M. *Science* **2009**, *326*, 1384−1387.
(45) Karunadasa, H. I.; Chang, C. J.; Long, J. R. *Nature* **2010**, *464*, 1329−1333.
(46) Helm, M. L.; Stewart, M. P.; Bullock, R. M.; Dubois, M. R.; Dubois, D. L. *Science* **2011**, *333*, 863−866.

DOI: 10.1021/cs501835c
ACS Catal. 2015, 5, 3801−3806